RSC Advances

PAPER

View Article Online
View Journal | View Issue

Cite this: *RSC Adv.*, 2017, **7**, 11503

Synthesis of In_2O_3 nanoparticle/TiO_2 nanobelt heterostructures for near room temperature ethanol sensing†

Yujie Li,‡ Hongru Yang,‡ Jian Tian,* Xiaolin Hu and Hongzhi Cui*

Received 1st January 2017
Accepted 7th February 2017

DOI: 10.1039/c7ra00011a

rsc.li/rsc-advances

In_2O_3 nanoparticle/TiO_2 nanobelt heterostructures are prepared *via* a facile hydrothermal strategy. Plenty of smaller In_2O_3 nanoparticles are uniformly deposited onto the surface of TiO_2 nanobelts. Compared with pure TiO_2 nanobelts and In_2O_3 nanoparticles, the obtained In_2O_3 nanoparticle/TiO_2 nanobelt heterostructures exhibit enhanced ethanol sensing properties at a temperature as low as 45 °C and a low detection limit (1 ppm). The improved sensing properties are mainly attributed to the synergic effect of fast charge transfer of heterostructure and the formation of preferential adsorption sites by the small size of the In_2O_3 nanoparticles.

Introduction

The growing concerns related to safety in residential areas resulted in the rapid development of the effective detection of toxic and hazardous gases.[1,2] As an important direct semiconductor with a band gap of 3.2 eV, TiO_2 has been applied in many fields of research, including solar cells,[3] Li-ion batteries,[4] photocatalysis,[5] photoelectrochemical cells,[6] and sensors,[7] due to its low cost and power consumption, ease of fabrication and use, stability in harsh environments, *etc.* Nanostructured TiO_2 is generally considered a remarkable candidate for gas sensors. However, the development of near room temperature/low detection limit gas sensors remains a challenge.

There are two common strategies that have been pursued in the literature to improve the properties of gas sensors.[8] One method is controlling the growth of TiO_2 with a specially designed shape and morphology, such as one-dimensional (1D) TiO_2 nanobelts.[9] Previous results have demonstrated that TiO_2 nanobelts are highly advantageous for use in chemical sensors comparing with their thin-film or bulk counterparts because of their high surface-to-volume ratio, controllable structure and facile electron transport in materials.[10] The other method is surface modification with semiconductor oxides, such as ZnO,[11] In_2O_3,[12] and Sn_3O_4,[8] to construct heterostructure. In gas sensing, the heterostructure acts as a lever in electron transfer, through which electron transfer is facilitated or restrained, resulting in the enhanced sensing properties of the sensor.

It is generally difficult for a gas sensor based on a single oxide semiconductor to satisfy all requirements on sensor response, selectivity, stability, and working temperature. Sensors based on two or more components have been explored to improve gas sensing performance.[13] Among the various oxides, 1D TiO_2, such as TiO_2 nanobelt, is a promising candidate as the backbone for the design and fabrication of composite nanostructures.[14] Indium oxide (In_2O_3), an n-type indirect band semiconductor with an indirect band gap of 2.8 eV, has been recognized as the potential sensing material due to its high electric conductance.[15] Other studies also show that In_2O_3 has high sensitivities to many gases such as H_2,[16] CO,[12] NO_2,[17] NH_3,[18] O_3,[19] and Cl_2.[20] In particular, In_2O_3-based sensors have been reported to be highly selective to ethanol gas.[15] However, the In_2O_3 nanoparticles have limited sensing activity due to the presence of fewer active surface sites inducing by aggregation. So In_2O_3 nanoparticles need to be well dispersed on the support to achieve high mass activity and resistance to aggregation. TiO_2 nanobelts possess a large surface area, and can provide sufficient space for the nucleation and growth of In_2O_3 nanoparticles on their surfaces. As motivated by the driving force of developing nanomaterials with

School of Materials Science and Engineering, Shandong University of Science and Technology, Qingdao 266590, China. E-mail: jiantian@sdust.edu.cn; cuihongzhi1965@163.com

† Electronic supplementary information (ESI) available: SEM image of TiO_2 nanobelts and surface-coarsened TiO_2 nanobelts; elemental energy-dispersive X-ray spectroscopy (EDS) mapping of the obtained In_2O_3 nanoparticle/TiO_2 nanobelt heterostructures (mole ratio 1 : 1), nitrogen adsorption–desorption isotherms of TiO_2 nanobelts, In_2O_3 nanoparticles and In_2O_3 nanoparticle/TiO_2 nanobelt heterostructures (mole ratio 1 : 1), In 3d and Ti 2p core-level XPS spectra of the samples, response of ethanol vapor sensors based on In_2O_3 nanoparticle/TiO_2 nanobelt heterostructures (mole ratio 1 : 1) upon exposure to 100 ppm of ethanol vapor at low operating temperature (45 °C, 55 °C and 80 °C), the sensing stability of the In_2O_3 nanoparticle/TiO_2 nanobelt heterostructures (mole ratio 1 : 1) sensor to 100 ppm ethanol with respect to a low temperature of 100 °C; UV-vis diffuse reflectance spectra of TiO_2 nanobelts, In_2O_3 nanoparticles and In_2O_3 nanoparticle/TiO_2 nanobelt heterostructures. Mott–Schottky plots of TiO_2 nanobelts and (c) In_2O_3 nanoparticles collected at a frequency of 1000 Hz in dark; zeta potentials of TiO_2 nanobelts and In_2O_3 nanoparticles in aqueous solution at different pH values. See DOI: 10.1039/c7ra00011a

‡ Theses authors contributed equally.

enhanced sensing performance, great efforts have been exhausted on the design of In_2O_3 nanoparticle/TiO_2 nanobelt heterostructures.

In this work, a novel heterostructure made of TiO_2 nanobelt backbones and small size of well-dispersed In_2O_3 nanoparticles is prepared by a facile hydrothermal method. Compared to pristine TiO_2 nanobelts and In_2O_3 nanoparticles, a near room temperature (45 °C)/low detection limit (1 ppm) gas sensing performance enhancement of In_2O_3 nanoparticle/TiO_2 nanobelt heterostructures is first documented. The TiO_2 nanobelt substrates restrict the growth of In_2O_3 nanoparticles, resulting in the formation of smaller In_2O_3 nanoparticles with more interaction sites for analytic gases. This remarkable property can be attributed to the combination of several factors, including efficient electron separation of heterostructure, increased surface active sites of In_2O_3 nanoparticles with small size, and the large surface area.

Materials and methods

Materials

Titania P25 (TiO_2), sodium hydroxide (NaOH), hydrochloric acid (HCl), sulfuric acid (H_2SO_4), indium nitrate hydrate ($In(NO_3)_3 \cdot 5H_2O$), carbamide ($CO(NH_2)_2$), diethylene glycol (DEG), and ethanol were purchased from Sinopharm.

Synthesis

Preparation of TiO_2 nanobelts. TiO_2 nanobelts were synthesized by a hydrothermal procedure. Typically, P25 powder (0.1 g) was mixed with an aqueous solution of NaOH (20 mL 10 M), followed by a hydrothermal treatment at 180 °C in a 25 mL Teflon-lined autoclave for 72 h. The treated powder was washed thoroughly with deionized water followed by filtration and drying processes. The obtained $Na_2Ti_3O_7$ nanobelts were then immersed in an aqueous solution of 0.1 M HCl for 48 h to obtained $H_2Ti_3O_7$ nanobelts. The above products were dissolved in a 0.02 M H_2SO_4 solution and maintained at 100 °C for 6 h. Finally, the products were isolated from solution by centrifugation and sequentially washed with deionized water several times by filtration, and dried at 60 °C for 10 h. Thermal annealing of the $H_2Ti_3O_7$ nanobelts by acid corrosion at 600 °C for 2 h led to production of TiO_2 nanobelts with roughened surfaces.

Preparation of In_2O_3 nanoparticle/TiO_2 nanobelt heterostructures (mole ratios at 1 : 2, 1 : 1 and 2 : 1). First, $In(NO_3)_3 \cdot 5H_2O$ (73.3–293 mg) and $CO(NH_2)_2$ (1 g) were dissolved in the mixture of 13 mL of diethylene glycol and 2 mL of H_2O under magnetic stirring. The TiO_2 nanobelts (15 mg) were dispersed in above solution with magnetically stirring for 2 h, and the final pH 6.5, then transferred into a 20 mL Teflon-lined stainless autoclave, sealed and maintained at 200 °C for 24 h. The as-fabricated products were collected out and washed several times with ethanol and deionized water by filtration, respectively. After drying at 60 °C for 12 h, the In_2O_3 nanoparticle/TiO_2 nanobelt heterostructures (mole ratios at 1 : 2, 1 : 1 and 2 : 1) were obtained. For comparison, pure In_2O_3 nanoparticles were also synthesized in the same manner without the addition of TiO_2 nanobelts.

Characterization. X-ray powder diffraction (XRD) patterns were recorded with a Bruke D8 Advance powder X-ray diffractometer with Cu Kα (λ = 0.15406 nm). Scanning electron microscopy (SEM) was performed with a FEI NanoSEM 450 instrument with an energy-dispersive X-ray spectroscopy (EDS). High resolution transmission electron microscopy (HRTEM) images were carried out with a JOEL JEM 2100F microscope. SEM and TEM samples were prepared by a drop casting method with 1 mg mL^{-1} ethanol solution of In_2O_3 nanoparticle/TiO_2 nanobelt heterostructures. X-ray photoelectron spectroscopy (XPS) was performed using an ESCALAB 250. The specific surface area was calculated using the Brunauer–Emmett–Teller (BET) method using the measurement instrument (Micromeritics, ASAP2020). The zeta potential of the samples suspended in deionized water was measured using a zeta potentiometer (Zetapals, Brookhaven).

Sensing tests. The gas sensing properties of as prepared TiO_2 nanobelts, In_2O_3 nanoparticles and In_2O_3 nanoparticle/TiO_2 nanobelt heterostructures were tested on a WS-30A gas sensing instrument (WeiSheng Electronics Co., Ltd., Henan, China). The fabrication and testing principle of gas sensors referred to previous works.[21] The response of the samples was defined as the ratio of R_a/R_g, where R_a and R_g are the electrical resistance of the sensor in air and in the presence of the test gas mixed in air, respectively.

Results and discussion

XRD analysis associated with TiO_2 nanobelts, In_2O_3 nanoparticles and In_2O_3 nanoparticle/TiO_2 nanobelt heterostructures is performed to investigate the crystal structure and purity of the samples, which is shown in Fig. 1. For TiO_2 nanobelts (curve a), eight distinctive peaks at 2θ = 25.3°, 37.8°,

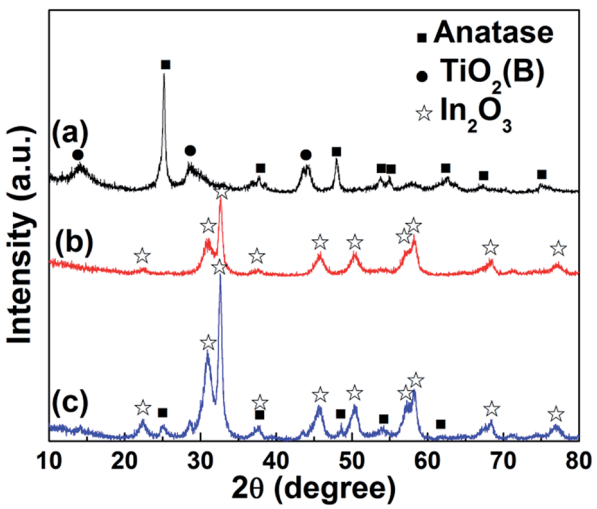

Fig. 1 XRD patterns of (a) TiO_2 nanobelts, (b) In_2O_3 nanoparticles, and (c) In_2O_3 nanoparticle/TiO_2 nanobelt heterostructures (mole ratio 1 : 1).

48.1°, 53.9°, 55.1°, 62.7°, 68.8°, and 76.0° match well with anatase TiO_2 (JCPDS 21-1272).[22] At the same time, the TiO_2(B) phase appears in the sample. The peak sites of TiO_2(B) locate at 14.2°, 28.5° and 43.5° (JCPDS 46-1237).[23] As shown in curve (b), the crystal phase of In_2O_3 nanoparticles with the diffraction peaks at about $2\theta = 22.4°$, 30.9°, 32.6°, 37.7°, 45.6°, 50.3°, 54.1°, 57.2°, 58.2° and 68.4°, which could be perfectly indexed to the (012), (104), (110), (113), (024), (116), (018), (214), (300) and (220) crystal faces of cubic In_2O_3 crystalline phase (JCPDS 71-2194).[24] For In_2O_3 nanoparticle/TiO_2 nanobelt heterostructures (curve c), all the peaks can be assigned to TiO_2 or In_2O_3, with no extra peaks observed, which demonstrates the high purity of the samples.

The size and morphology of samples were investigated by scanning electron microscopy (SEM), as exhibited in Fig. 2 and S1.† The as-obtained TiO_2 nanobelts are around 200 nm in width, 20–40 nm in thickness, and several micrometers in length[25] (Fig. S1a†). After the acid etching process, the surface-coarsened TiO_2 nanobelts are obtained (Fig. S1b and c†), which have a large specific surface area and can offer abundant nucleation sites for the deposition of In_2O_3 nanoparticles.[10] Fig. 2a reveals an agglomeration of individual In_2O_3 nanoparticles. The successful formation of In_2O_3 nanoparticle/TiO_2 nanobelt heterostructures is confirmed by the SEM image (Fig. 2b). The TiO_2 nanobelts are homogeneously covered by numerous In_2O_3 nanoparticles with several nanometers in size. It is the coarsened surface of TiO_2 nanobelts that prevents In_2O_3 nanoparticles forming aggregation in the reaction procedure. The formed heterostructure can improve the efficiency of interfacial charge separation and enhance the gas sensing activity.[26] Besides, the very small size of the In_2O_3 nanoparticles could lead to highly sensitive sensors because of the high sensing surface.[27] EDS mapping (Fig. S2†) also shows that In, Ti, and O elements are found in the In_2O_3 nanoparticle/TiO_2 nanobelt heterostructures, and no other impurities are observed.

N_2 isotherms adsorption–desorption curves are used to determine specific surface areas (Fig. S3†). The In_2O_3 nanoparticle/TiO_2 nanobelt heterostructures with rough surface generally have a higher specific surface area (43.357 $m^2\ g^{-1}$) than In_2O_3 nanoparticles (39.356 $m^2\ g^{-1}$) and TiO_2 nanobelts (32.767 $m^2\ g^{-1}$), which is favorable for gas detection. The large contact area can provide more reaction surface between heterostructure and target gas, resulting in the enhancement of gas sensing performance.

Fig. 3 shows the typical TEM images of In_2O_3 nanoparticle/TiO_2 nanobelt heterostructures. It can be seen that the In_2O_3 nanoparticles with size of *ca.* 10–15 nm are attached on the surface of TiO_2 nanobelts (Fig. 3a and b), coinciding with the results from the SEM observations. The crystalline lattice for the nanoparticle displays a *d*-spacing of approximately 0.29 nm, which corresponds to the interplanar spacing of the (222) planes of cubic In_2O_3 (Fig. 3c).[28] In addition, the spacing of the fringes in the brighter region are 0.35 nm, which are assigned to the interplanar spacing of the (110) planes of TiO_2 (Fig. 3c).[29] The HRTEM images (Fig. 3c) clearly confirm that the In_2O_3 nanoparticle/TiO_2 nanobelt heterostructure has been fabricated successfully through as-adopted hydrothermal strategy. Such a close contact is expected to favor an efficient charge transfer between In_2O_3 and TiO_2, inducing a faster response of the sensor.

The XPS measurement of In_2O_3 nanoparticle/TiO_2 nanobelt heterostructures is performed to further confirm the chemical composition and oxidation state, and the results are shown in Fig. 4. The fully scanned spectrum of In_2O_3 nanoparticle/TiO_2 nanobelt heterostructures suggests that the sample consists of In, Ti, O and C, as shown in Fig. 4a. The elements of In, Ti, and O belong to the In_2O_3 nanoparticle/TiO_2 nanobelt heterostructure. The peak for C 1s at 284.8 eV is ascribed to adventitious carbon from the XPS instrument.[30] The XPS spectrum (Fig. 4b) for Ti 2p shows two peaks at 464.2 and 458.5 eV that are assigned to Ti $2p_{1/2}$ and Ti $2p_{3/2}$ respectively, which is a characteristic of Ti^{4+} in TiO_2.[31] The In 3d XPS spectrum (Fig. 4c) consists of two peaks centered at 452.5 and 444.5 eV for the $3d_{3/2}$ and $3d_{5/2}$ peaks, respectively, corresponding to the In^{3+} spectrum in In_2O_3.[32] The O 1s spectrum shows three peaks at 529.6, 531.2 and 532.0 eV, as shown in Fig. 4d. Here, the intense peaks at 529.6 and 531.2 eV can be assigned to lattice oxygen in TiO_2 and In_2O_3 species, whereas the weak peak at 532 eV is possibly related to the adsorbed oxygen.[33] All of these results give the insight that the In_2O_3 nanoparticle/TiO_2 nanobelt heterostructures are composed of In_2O_3 and TiO_2. Moreover, the In 3d peaks in the In_2O_3 nanoparticle/TiO_2 nanobelt heterostructures shift toward the higher binding energies as compared with those of pure In_2O_3, while lower binding energies of Ti 2p from TiO_2 are observed in the heterostructure (Fig. S4†). These phenomena can be explained by partial electron transfers from In_2O_3 to TiO_2, *i.e.*, an increase (decrease) of the electron density of TiO_2 (In_2O_3) leads to the reduction (enhancement) of the binding energies of Ti 2p (In 3d). From the XPS results, we can expect the strong interfacial coupling effect between In_2O_3 and TiO_2, which could promote the electron transfer and further enhance the gas sensing performance of In_2O_3 nanoparticle/TiO_2 nanobelt heterostructures.

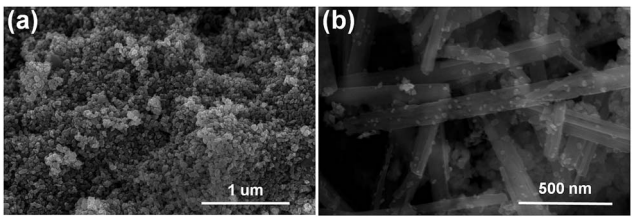

Fig. 2 SEM image of (a) In_2O_3 nanoparticles and (b) In_2O_3 nanoparticle/TiO_2 nanobelt heterostructures (mole ratio 1 : 1).

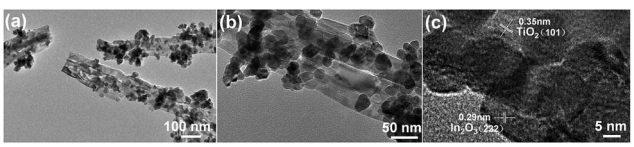

Fig. 3 (a and b) TEM and (c) high-magnification TEM images of In_2O_3 nanoparticle/TiO_2 nanobelt heterostructures (mole ratio 1 : 1).

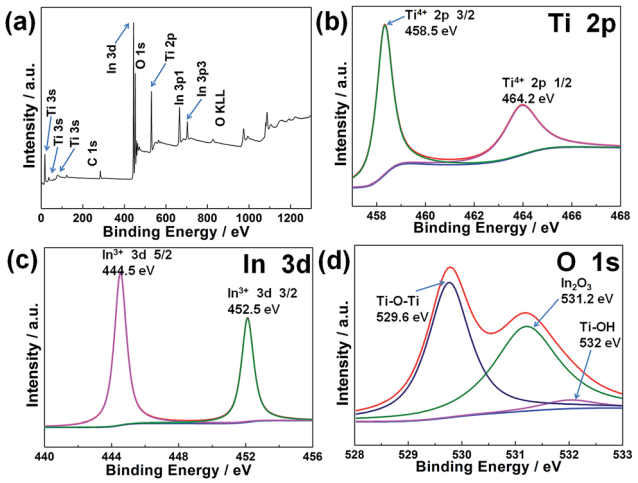

Fig. 4 XPS spectra of In_2O_3 nanoparticle/TiO_2 nanobelt heterostructures (mole ratio 1 : 1): (a) fully scanned spectra, (b) Ti 2p, (c) In 3d, and (d) O 1s.

The schematic of the ethanol gas sensor is shown in Fig. 5a. The relationship between the operating temperature and gas responses to 100 ppm ethanol of the three kinds of sensor devices were first investigated in the temperature range of 45–440 °C (Fig. 5b and S5†). Since the target gas molecules are not active enough to overcome the activation energy barrier to react with the surface-absorbed oxygen species at a low temperature,[34–37] while at temperatures that are too high and difficult in gas adsorption, in turn cause the low utilization rate of the sensing material; thus, low gas responses are achieved in both of two situation.[38] Hence, an "increase-maximum-decay" tendency is obtained along with the temperature increasing. More noticeable, it can be seen that TiO_2 nanobelts, In_2O_3 nanoparticles, and In_2O_3 nanoparticle/TiO_2 nanobelt heterostructures share the same optimal operating temperature at about 400 °C. The sensor response of the pure TiO_2 nanobelts and In_2O_3 nanoparticles is only 10.2 and 63.8, respectively at 400 °C. The response of the sensor based on In_2O_3 nanoparticle/TiO_2 nanobelt heterostructures reaches a maximum value of 106.3 at 400 °C, which was 1.67 times and 10.4 times higher than that of In_2O_3 nanoparticles and TiO_2 nanobelts, respectively. Even at operating temperature as low as 100 °C (Fig. 5b), the sensitivity of the In_2O_3 nanoparticle/TiO_2 nanobelt heterostructures reaches to about 13, which is much higher than those listed in literatures.[39,40] Moreover, the In_2O_3 nanoparticle/TiO_2 nanobelt heterostructures still have response even at near room temperature (45 °C) (Fig. S5†). To the best of our knowledge, this remarkable response to ethanol and selectivity at 45 °C has never reported before for an In_2O_3 based sensor. Thus, it is a proof of concept that In_2O_3 nanoparticle/TiO_2 nanobelt heterostructures can be used as selective sensor at near room temperature.

The dynamic responses of TiO_2 nanobelts, In_2O_3 nanoparticles and In_2O_3 nanoparticle/TiO_2 nanobelt heterostructures under different concentration from 1 ppm to 100 ppm of ethanol at an optimal operating temperature of 400 °C are revealed in Fig. 6. It can be seen that the corresponding responses of the sensors are highly dependent on the concentration of ethanol. The sensor made from the In_2O_3 nanoparticle/TiO_2 nanobelt heterostructures even shows a higher response (21) at 10 ppm, which is better than that of TiO_2 nanobelts and In_2O_3 nanoparticles, indicating the good sensing capability to ethanol (Fig. 6a–c). Impressively, the In_2O_3 nanoparticle/TiO_2 nanobelt heterostructures still have the response at the very low concentration of 1 ppm (Fig. 6d).

From the perspective of practical application of sensor device, not only high response but also fast response speed should be paid attention to, on account of their vital roles on avoiding possible loss and disasters. The dynamic response curve shown in Fig. 6a–c demonstrates the In_2O_3 nanoparticle/TiO_2 nanobelt heterostructures exhibit excellent response and recovery capability toward 100 ppm ethanol. The response time of In_2O_3 nanoparticle/TiO_2 nanobelt heterostructures to 100 ppm ethanol is as low as 6 s, which is far less than that of In_2O_3 nanoparticles (9 s) and TiO_2 nanobelt (21 s). Meanwhile, the recovery time of the In_2O_3 nanoparticle/TiO_2 nanobelt heterostructures, In_2O_3 nanoparticles and TiO_2 nanobelts are 3 s, 4 s and 45 s to 100 ppm ethanol, respectively. Therefore, the In_2O_3 nanoparticle/TiO_2 nanobelt heterostructure sensor

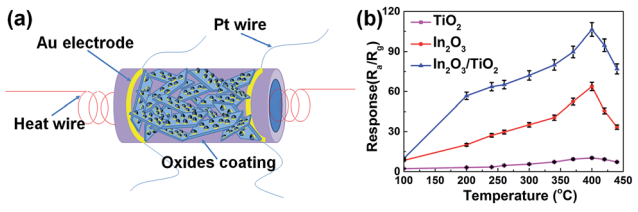

Fig. 5 (a) Schematic of the ethanol gas sensor; (b) variation of response (R_a/R_g) with working temperature of the three different kinds of sensors based on TiO_2 nanobelts, In_2O_3 nanoparticles, and In_2O_3 nanoparticle/TiO_2 nanobelt heterostructures (mole ratio 1 : 1) to 100 ppm ethanol vapor.

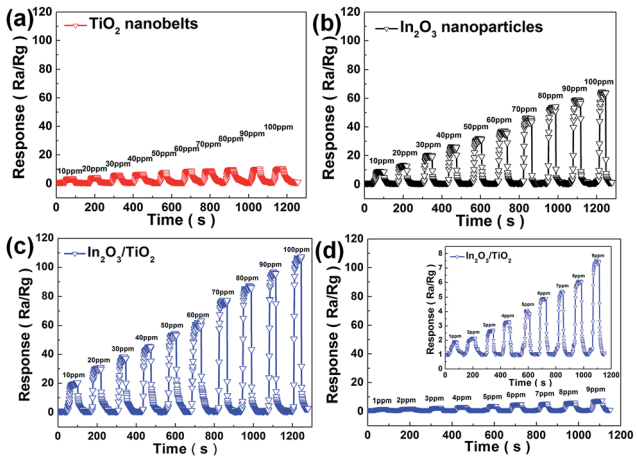

Fig. 6 Response curve and response profiles of ethanol vapor sensors based on (a) TiO_2 nanobelts, (b) In_2O_3 nanoparticles, and (c and d) In_2O_3 nanoparticle/TiO_2 nanobelt heterostructures (mole ratio 1 : 1) upon exposure to different concentrations of ethanol vapor at an optimal operating temperature of 400 °C.

displays faster response and recovery speed than pristine In_2O_3 nanoparticle and TiO_2 nanobelt.

Since selectivity is a remarkable aspect of sensing properties. Fig. 7 reveals the response of the sensor that coating In_2O_3 nanoparticle/TiO_2 nanobelt heterostructures to various kinds of test gases (acetone, benzene, ammonium hydroxide, ethyl acetate and ethanol) at 100 ppm. All of those gases are tested at a low temperature of 100 °C. Obviously, the response to ethanol is much higher than that of other probe analytes, suggesting good selectivity of as prepared In_2O_3 nanoparticle/TiO_2 nanobelt heterostructures.

It should be noted that the sensing activity of In_2O_3 nanoparticle/TiO_2 nanobelt heterostructures also depend on the In_2O_3 : TiO_2 molar ratio, as shown in Fig. 7. All of the In_2O_3 nanoparticle/TiO_2 nanobelt heterostructures at different mole ratios present excellent response to ethanol at a low temperature of 100 °C, which can be explained that the high dispersed In_2O_3 nanoparticles on the surface of TiO_2 nanobelts will have good sensing activity. The optimal molar ratio of In_2O_3 : TiO_2 is 1 : 1. The In_2O_3 nanoparticle/TiO_{2p} nanobelt heterostructures at mole ratio (1 : 2) exhibit lower ethanol response due to the less amount of In_2O_3 and low number of junctions with TiO_2 nanobelts. Moreover, the In_2O_3 nanoparticle/TiO_2 nanobelt heterostructures at mole ratio (1 : 1) present higher ethanol response than that of In_2O_3/TiO_2 mole ratio (2 : 1). This should be caused that excessive In_2O_3 nanoparticles cover the active sites of TiO_2 nanobelts, which hinder the electron transfer on the interface of In_2O_3 nanoparticle/TiO_2 nanobelt heterostructures, and thus in turn inhibit the sensing activity.

The cyclic experiment on sensing performance of In_2O_3 nanoparticle/TiO_2 nanobelt heterostructures proves that the heterostructures display excellent ethanol response stability even after 6 weeks (Fig. S6†).

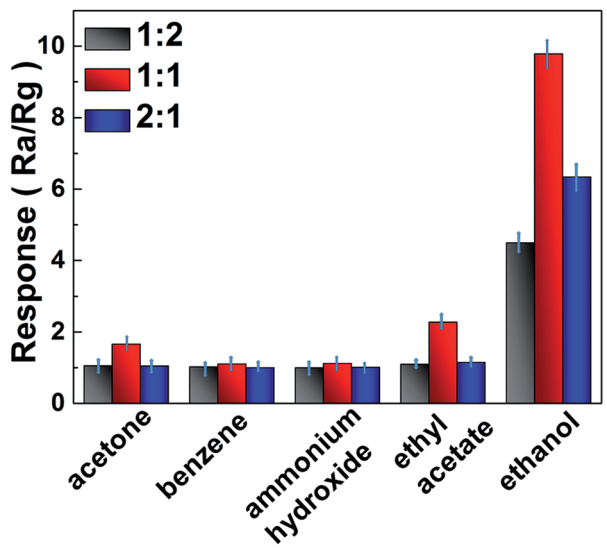

Fig. 7 Response (R_a/R_g) of In_2O_3 nanoparticle/TiO_2 nanobelt heterostructures (mole ratio at 1 : 2, 1 : 1, and 2 : 1) sensor to acetone, benzene, ammonium hydroxide, ethyl acetate and ethanol vapor at 100 ppm with respect to a low temperature of 100 °C.

On the basis of the above results, a synergetic mechanism between In_2O_3 nanoparticles and TiO_2 nanobelts in the In_2O_3 nanoparticle/TiO_2 nanobelt heterostructures for the enhanced gas sensing property is proposed (Fig. 8). The conducted band (CB) and valence band (VB) potentials of In_2O_3 nanoparticles are estimated to be −0.63 and +2.17 eV, and the CB and VB of TiO_2 nanobelts are at −0.4 and +2.8 eV, respectively (Fig. S7†).[26,39–43]

To further explain the mechanism of the reactions between In_2O_3 nanoparticle/TiO_2 nanobelt heterostructures and the target gas ethanol, a rational model is proposed, as shown in Fig. 8a and b. It has been clearly revealed that the In_2O_3 nanoparticles decorated TiO_2 nanobelts nanostructure exhibit much better sensing performances than that of pure In_2O_3 nanoparticles and TiO_2 nanobelts, indicating the formation of heterostructure, which can contribute greatly to the improvement of sensing properties. The dramatic enhancement in sensing properties of In_2O_3 nanoparticle/TiO_2 nanobelt heterostructures can be attributed to the following three factors.

First, the striking synergistic effect of the two metal oxides. For the as-prepared In_2O_3 nanoparticle/TiO_2 nanobelt heterostructures, the surfaces of TiO_2 nanobelts are not completely enclosed by In_2O_3 nanoparticles, resulting in both of them being highly accessible for the adsorption of oxygen molecules and promoting the formation of depletion layers on the surfaces of both metal oxides while exposed to air.[44–47] Therefore, both In_2O_3 nanoparticles and TiO_2 nanobelts contribute to ethanol response.

Second, preparation of small and well-dispersed sensing materials is an effective manner to improve the sensor response. In the current work, well-dispersed In_2O_3 nanoparticles are deposited onto the surface of TiO_2 nanobelts through controlling pH = 6.5 to keep strong electrostatic attraction between TiO_2 and In_2O_3 (Fig. S8†). The TiO_2 nanobelts can act as backbone for the nucleation and growth of In_2O_3 nanoparticles,[48] and prevent the aggregation of In_2O_3 nanoparticles. The smaller In_2O_3 nanoparticles on the surface

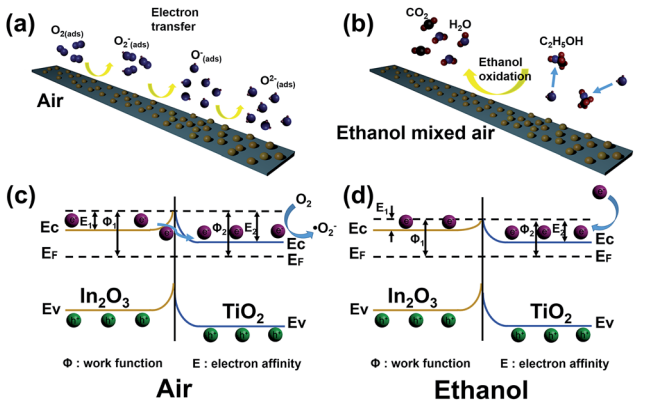

Fig. 8 Model of the sensor based on In_2O_3 nanoparticle/TiO_2 nanobelt heterostructures exposed in (a) air and (b) ethanol mixed air, respectively; (c and d) gas sensing mechanism of In_2O_3 nanoparticle/TiO_2 nanobelt heterostructures, E_c: conduction band, E_F: Fermi level and E_v: valence band.

of TiO_2 nanobelts have the exposure of more sensitive surfaces, and can serve as effective adsorption sites to bind and activate oxygen molecules. Thus, more absorbed oxygen species will diffuse to the surface of the sensing semiconductor, resulting in a larger degree of electron extractions from the conduction band of TiO_2 nanobelts. The high coverage of chemisorbed oxygen species make the In_2O_3 nanoparticle/TiO_2 nanobelt heterostructures more sensitive to ethanol, directly resulting in a high response.

More importantly, owing to the strong electronic interaction between In_2O_3 nanoparticles and TiO_2 nanobelts, a typical semiconductor junction was formed. The charge transport is significantly enhanced in the heterostructure, resulting in a rapid response–recovery.[49] So, the In_2O_3 nanoparticle/TiO_2 nanobelt heterostructures are more sensitive to target gas and have superior properties.

Fig. 8c and d show the energy band diagram near the In_2O_3 nanoparticle/TiO_2 nanobelt heterostructures. When the n-type semiconductor In_2O_3 nanoparticles and n-type semiconductor TiO_2 nanobelts contact with each other, electrons would transfer from the CB of In_2O_3 to the CB of TiO_2 until the Fermi energy levels (E_F) of them become equal[50] (Fig. 8c). In ambient air, sensing materials can absorb oxygen molecules (O_2) and form surface-adsorbed oxygen species ($O_{2(ads)}^-$, $O_{(ads)}^-$, and $O_{(ads)}^{2-}$, eqn (1)–(4)) by capturing free electrons from the CB of In_2O_3 nanoparticles. The reaction kinematics can be described as follows:[25]

$$O_{2(g)} \rightarrow O_{2(ads)} \quad (1)$$

$$O_{2(ads)} + e^- \rightarrow O_{2(ads)}^- \quad (2)$$

$$O_{2(ads)}^- + e^- \rightarrow 2O_{(ads)}^- \quad (3)$$

$$O_{(ads)}^- + e^- \rightarrow O_{(ads)}^{2-} \quad (4)$$

In this process, a thick electron depletion layer formed on the surface area, resulting in a decrease of carrier concentration and increase of sensor resistance in coincidence.[51] When the sensor is exposed to ethanol, at a moderate temperature, the adsorbed oxygen species will take part in the reaction with these gas molecules to form CO_2 and H_2O (eqn (5)). The reactions between reducing gases and the surface adsorbed oxygen species can be described as follows:

$$C_2H_5OH + 6O_{(ads)}^- \rightarrow 2CO_2 + 3H_2O + 6e^- \quad (5)$$

As a result, the electrons trapped in the ionized oxygen species are released back to the CB of In_2O_3 nanoparticles (Fig. 8d), which eventually lead to the thickness of electron depletion layer decreases and lowering the measured resistance of the sensor.

Conclusions

Unique 1D nanostructures of TiO_2 decorated with In_2O_3 nanoparticles have been synthesized *via* a simple hydrothermal method. The TiO_2 nanobelt substrates restrict the growth of In_2O_3 nanoparticles, resulting in the formation of uniform and smaller In_2O_3 nanoparticles with a high number of surface active sites. Notably, the obtained In_2O_3 nanoparticle/TiO_2 nanobelt heterostructures exhibit a much higher sensitive toward ethanol at near room temperature of 45 °C and low detection limit of 1 ppm. The synergic effect of pronounced electron transfer of heterostructure, as well as the creation of active adsorption sites by the small size of In_2O_3 nanoparticles result in an enhancement of gas response in terms of response, response/recovery time and selectivity toward ethanol.

Acknowledgements

The authors are thankful for fundings from the National Natural Science Foundation of China (No. 51502160 and 51272141), National High Technology Research and Development Program of China (No. 2015AA034404), Taishan Scholar Climbing Plan of Shandong Province, Natural Science Foundation of Shandong Province (No. ZR2015EQ001), Applied Basic Research Foundation of Qingdao City (No. 16-5-1-93-jch), and SDUST Research Fund (No. 2015JQJH101).

Notes and references

1 S. Ghosh, N. A. Kouamé, L. Ramos, S. Remita, A. Dazzi, A. Deniset-Besseau, P. Beaunier, F. Goubard, P. H. Aubert and H. Remita, *Nat. Mater.*, 2015, **14**, 505–511.
2 X. Liang, T.-H. Kim, J.-W. Yoon, C.-H. Kwak and J.-H. Lee, *Sens. Actuators, B*, 2015, **209**, 934–942.
3 T. Kitamura, M. Ikeda, K. Shigaki, T. Inoue, N. A. Anderson, X. Ai, T. Lian and S. Yanagida, *Chem. Mater.*, 2004, **16**, 1806–1812.
4 F. Cao, X. Wu, S. Xin, Y. Guo and L. Wan, *J. Phys. Chem. C*, 2010, **114**, 10308–10313.
5 Y. Zhang, Z. Tang, X. Fu and Y. Xu, *ACS Nano*, 2011, **5**, 7426–7435.
6 T. Stergiopoulos, I. M. Arabatzis, G. Katsaros and P. Falaras, *Nano Lett.*, 2002, **2**, 1259–1261.
7 C. Wang, L. Yin, L. Zhang, Y. Qi, N. Lun and N. Liu, *Langmuir*, 2010, **26**, 12841–12848.
8 G. Chen, S. Ji, H. Li, X. Kang, S. Chang, Y. Wang, G. Yu, J. Lu, J. Claverie and Y. Sang, *ACS Appl. Mater. Interfaces*, 2015, **7**, 24950–24956.
9 A. Hazra, B. Bhowmik, K. Dutta, P. Chattopadhyay and P. Bhattacharyya, *ACS Appl. Mater. Interfaces*, 2015, **7**, 9336–9348.
10 P. Hu, G. Du, W. Zhou, J. Cui, J. Lin, H. Liu, D. Liu, J. Wang and S. Chen, *ACS Appl. Mater. Interfaces*, 2010, **2**, 3263–3269.
11 C. Wang, L. Yin, L. Zhang, D. Xiang and R. Gao, *Sensors*, 2010, **10**, 2088–2106.
12 N. Singh, R.-K. Gupta and P.-S. Lee, *ACS Appl. Mater. Interfaces*, 2011, **3**, 2246–2252.
13 B. Wu, Z. Lin, M. Sheng, S. Hou and J. Xu, *Appl. Surf. Sci.*, 2016, **360**, 652–657.
14 J. Tian, Z. Zhao, A. Kumar, R. I. Boughton and H. Liu, *Chem. Soc. Rev.*, 2014, **43**, 6920–6937.

15 S. Park, S. Kim, G.-J. Sun and C. Lee, *ACS Appl. Mater. Interfaces*, 2015, **7**, 8138–8146.
16 A. Qurashi, E. El-Maghraby, T. Yamazaki and T. Kikuta, *Sens. Actuators, B*, 2010, **147**, 48–54.
17 S. Elouali, L. G. Bloor, R. Binions, I. P. Parkin, C. J. Carmalt and J. A. Darr, *Langmuir*, 2012, **28**, 1879–1885.
18 G. W. Ho, *Sci. Adv. Mater.*, 2011, **3**, 150–168.
19 X. Lu, Q. Yu, K. Wang, L. Shi, X. Liu, A. Qiu, L. Wang and D. Cui, *Cryst. Res. Technol.*, 2010, **45**, 557–561.
20 Y. Zhang, G. Jiang, K. W. Wong and Z. Zheng, *Sens. Lett.*, 2010, **8**, 355–361.
21 X. Wang, S. Qiu, J. Liu, C. He, G. Lu and W. Liu, *Eur. J. Inorg. Chem.*, 2014, **2014**, 863–869.
22 J. Tian, P. Hao, N. Wei, H. Cui and H. Liu, *ACS Catal.*, 2015, **5**, 4530–4536.
23 W. Zhou, G. Du, P. Hu, G. Li, D. Wang, H. Liu, J. Wang, R. I. Boughton, D. Liu and H. Jiang, *J. Mater. Chem. A*, 2011, **21**, 7937–7945.
24 K. Nouneh, M. Oyama, R. Diaz, M. Abd-Lefdil, I. V. Kityk and M. Bousmina, *J. Alloys Compd.*, 2011, **509**, 2631–2638.
25 X. Wang, Y. Sang, D. Wang, S. Ji and H. Liu, *J. Alloys Compd.*, 2015, **639**, 571–576.
26 J. Tian, Y. Sang, Z. Zhao, W. Zhou, D. Wang, X. Kang, H. Liu, J. Wang, S. Chen and H. Cai, *Small*, 2013, **9**, 3864–3872.
27 T.-T. Trinh, N.-H. Tu, H.-H. Le, K.-Y. Ryu, K.-B. Le, K. Pillai and J. Yi, *Sens. Actuators, B*, 2011, **152**, 73–81.
28 J. Luo, X. Zhou, L. Ma, X. Xu, H. Ruan and Z. Zhang, *RSC Adv.*, 2016, **6**, 52627–52635.
29 Q. Li, T. Li, S. Chang, Q. Tao, B. Tian and J. Zhang, *CrystEngComm*, 2016, DOI: 10.1039/c6ce00938g.
30 S. Gao, C. Dong, L. Hong, K. Xiao, X. Pan and X. Li, *Electrochim. Acta*, 2013, **114**, 233–241.
31 L. Ma, M. Hou, Z. Xie and Z. Zhang, *Sci. Rep.*, 2015, **5**, 12890.
32 L. Lin, J. Yu, S. Cheng and P. Lu, *Chin. Phys. B*, 2015, **24**, 078103.
33 J. G. Kim, D. L. Pugmire, D. Battaglia and M. A. Langell, *Appl. Surf. Sci.*, 2000, **165**, 70–84.
34 R. Asapu, V. M. Palla, B. Wang, Z. Guo, R. Sadu and D. H. Chen, *J. Photochem. Photobiol., A*, 2011, **225**, 81–87.
35 C. Jin, K. Baek, H. Kim and C. Lee, *Curr. Appl. Phys.*, 2011, **11**, S274–S278.
36 L. Zhang, K. Wong, H. Yip, C. Hu, J. Yu, C. Chan and P. Wong, *Environ Sci Tech*, 2010, **44**, 1392–1398.
37 R. Bari, P. Patil, S. Patil and A. Bari, *Bull. Mater. Sci.*, 2013, **36**, 967–972.
38 J. Liu, M. Dai, T. Wang, P. Sun, X. Liang, G. Lu, K. Shimanoe and N. Yamazoe, *ACS Appl. Mater. Interfaces*, 2016, **8**, 6669–6677.
39 X. Li, J. Liu, H. Guo, X. Zhou, C. Wang, P. Sun, X. Hu and G. Lu, *RSC Adv.*, 2015, **5**, 545–551.
40 T. Zhang, F. Gu, D. Han, Z. Wang and G. Guo, *Sens. Actuators, B*, 2013, **177**, 1180–1188.
41 J. Zai, J. Zhu, R. Qi and X. Qian, *J. Mater. Chem.*, 2013, **1**, 735–745.
42 Z. Zhao, D. Wang, X. Kang, Y. Sang and H. Liu, *Energy and Environment Focus*, 2014, **3**, 404–410.
43 J. Lv, T. Kako, Z. Li, Z. Zou and J. Ye, *J. Phys. Chem. C*, 2010, **114**, 6157–6162.
44 Y. Wang, Q. Wang, X. Zhan, F. Wang, M. Safdar and J. He, *Nanoscale*, 2013, **5**, 8326–8339.
45 S. Mubeen, G. Hernandez-Sosa, D. Moses, J. Lee and M. Moskovits, *Nano Lett.*, 2011, **11**, 5548–5552.
46 J. Mu, B. Chen, M. Zhang, Z. Guo, P. Zhang, Z. Zhang, Y. Sun, C. Shao and Y. Liu, *ACS Appl. Mater. Interfaces*, 2011, **4**, 424–430.
47 P. Feng, Q. Wan and T. Wang, *Appl. Phys. Lett.*, 2005, **87**, 213111.
48 G. Chen, S. Ji, Y. Sang, S. Chang, Y. Wang, P. Hao, J. Claverie, H. Liu and G. Yu, *Nanoscale*, 2015, **7**, 3117–3125.
49 T. Kirchartz, W. Gong, S. A. Hawks, T. Agostinelli, R. C. MacKenzie, Y. Yang and J. Nelson, *J. Phys. Chem. C*, 2012, **116**, 7672–7680.
50 S. Xu, J. Gao, L. Wang, K. Kan, Y. Xie, P. Shen, L. Li and K. Shi, *Nanoscale*, 2015, **7**, 14643–14651.
51 R. Sharma, S. Patel and K. Pargaien, *Adv. Nat. Sci.: Nanosci. Nanotechnol.*, 2012, **3**, 035005.